Physical Consistency of Giant Permittivity in Humid Nanostructured Silica Capacitors via Kramers-Kronig Analysis

Bremnen Véliz *, Sendey Vera , Sandra Bermejo , Albert Orpella , Manuel Domínguez-Pumar

Posted Date: 23 March 2026

doi: 10.20944/preprints202603.1699.v1

Keywords: Kramers-Kronig; nanostructured silica; humidity dependence; metal-insulator-metal capacitor; electronic and ionic conduction

 doi:10.20944/preprints202603.1699.v1

Article

Physical Consistency of Giant Permittivity in Humid Nanostructured Silica Capacitors via Kramers-Kronig Analysis

Bremnen Véliz [1,*], Sendey Vera [1], Sandra Bermejo [2], Albert Orpella [2] and Manuel Domínguez-Pumar [2]

[1] Universidad Estatal Península de Santa Elena

[2] Universitat Politécnica de Catalunya

* Correspondence: bveliz@upse.edu.ec

Highlights

What are the main findings?

- Kramers-Kronig analysis demonstrates that giant permittivity in nanostructured silica metal-insultar-metal capacitors is extrinsic, arising from humidity-induced deviations in linearity and causality.
- Augmented transmission line modeling identifies moisture-driven ionic conduction and interfacial polarization as the specific mechanisms causing impedance consistency breakdown at relative humidity.

What are the implications of the main findings?

- Violations of Kramers-Kroning relations serve as diagnostic signatures of ionic transport mechanism rather than indicators of data reliability issues in porous dielectrics.
- The strong humidity dependence validates electrosprayed silica nanoparticles as high-performance sensing materials, while highlighting environment constraints for stable capacitor applications.

Abstract

Metal-Insulator-Metal (MIM) capacitors based on electrosprayed silica nanoparticles exhibit giant effective permittivity, making them attractive for miniaturized capacitive and sensing. However, their dielectrics response is highly sensitive to ambient humidity, which can compromise data reliability. This study analyzes impedance characteristics of two silica nanoparticles-based MIM capacitors: (i) one measured under ambient conditions across 0.1Hz to 2MHz at 100mV and 500mV excitation, and (ii) another characterized under controlled relative humidity (RH) conditions (40%, 70% and 90%). The physical consistency of the measured impedance is rigorously assessed via Kramers-Kronig (KK) transforms. The first capacitor shows excellent KK consistency for the real part of the impedance (NRMSE=3.3%), indicating behavior compatible with linear-invariant assumptions. In contrast, the second capacitor exhibits strong humidity dependence deviations, NRMSE for Z' rises from 14.5% at 40%RH to 141.2% at 90%RH, suggesting a breakdown of linearity and causality due to moisture-induced ionic conduction and interfacial polarization processes. These findings demonstrate that while increased humidity amplifies the effective dielectric response, it simultaneously introduces non-ideal effects that invalidate standard KK assumptions. This work underscores the necessity of environmental control and provide critical insights for the design of humidity-sensitive devices and stable insulating capacitors.

Keywords: Kramers-Kronig; nanostructured silica; humidity dependence; metal-insulator-metal capacitor; electronic and ionic conduction

 doi:10.20944/preprints202603.1699.v1

1. Introduction

Metal–insulator–metal (MIM) capacitors based on nanostructured dielectrics have attracted significant interest due to their potential for high capacitance density, and integration in modern microelectronic and sensing systems [1–6]. Among these, electrosprayed silica (SiO_2) nanoparticle structures [7] have demonstrated exceptionally high effective permittivity— three orders of magnitude larger than that of bulk SiO_2—making them promising candidates for energy storage and environmental sensing applications. The electrosprayed porous shape layer, which encourages interfacial polarization and strong field confinement at the nanoscale, is responsible for this increased sensitivity.

However, environmental factors such as relative humidity and temperature, have a significant impact on the electrical impedance spectroscopy [8] behavior of nanostructured silica capacitors [9]. The water molecules adsorbed into the nanopores can dissociate into mobile ions, introducing ionic conductivity that substantially alter the impedance response [10]. While the capacitive response and equivalent-circuit modeling of electrosprayed SiO_2 structures have been previously reported for similar devices [11], the physical reliability of the impedance data—particularly under controlled humidity—and the underlying mechanisms governing the observed giant permittivity remain unexplored.

Kramers-Kronig (KK) relations are frequently used to evaluate the physical validity of the measured impedance data. Without the need for an equivalent circuit model, the KK relations [12] offer a rigorous framework to verify whether experimental impedance data meet linearity, causality, and stability [13] requirements. In the absence of KK criteria, equivalent circuit models may yield misleading parameters or questionable impedance data. While practical implementations may require data extrapolation, sometimes assisted by equivalent circuit models, the core validation is based on the mutual consistency between the real and imaginary parts of the impedance [14].

This work addresses this gap by looking at Kramers–Kronig analysis, which serves not as a just pass/fail test, but as a diagnostic tool to reveal the extrinsic origins of the dielectric enhancement. Although Kramers–Kronig relations are often used as a consistency check in impedance spectroscopy, deviations from KK relations do not necessarily imply a problem of the quality of the experimental data. Instead, they may reveal hidden non-idealities such as time-dependent ionic transport, interfacial polarization, or environmental coupling, which are particularly relevant in nanostructured dielectric materials.

In this study, we investigate the impedance characteristics of two distinct electrosprayed SiO_2 MIM capacitors: one was characterized in regular ambient laboratory conditions with ambient air, and another tested under specific controlled relative humidity levels (40%, 70%, and 90%). To apply the KK transform, we use the discretized formulation proposed by Agarwal, Orazem, and García-Rubio [15], which accounts for the high-frequency limit and keeps numerical stability. Our analysis demonstrates that while the ambient-condition device exhibits excellent KK consistency, the humidity-exposed capacitor shows increasing deviation with rising moisture content which appears to be linked to ionic conduction plus interfacial polarization.

2. Materials and Methods

2.1. Fabrication of Electrosprayed SiO_2 Nanostructures

The silica nanoparticles, dispersed in colloidal fluid consisting of 95% deionized water and 5% solid content, were purchased from microParticles GmbH. Two metal-insulator-metal (MIM) capacitors were fabricated on a glass substrate by electrospraying a layer of 255-nm SiO_2 nanoparticles as dielectric, with aluminum top and bottom electrodes defined by standard microfabrication. Both devices had an active electrode area of 3.24 mm^2 and 15.9 mm^2. Full fabrication details are provided [10].

2.2. Characterization

 doi:10.20944/preprints202603.1699.v1

Impedance spectroscopy measurements were performed using a Hioki IM3590 (from 0.1 Hz to 100 kHz) and a 4294A semiconductor analyzer (from 100 kHz to 2 MHz). Two measurement protocols were followed:

Capacitor 1: Characterized under ambient laboratory conditions (uncontrolled humidity), with the excitation voltage of 100 mV and 500 mV.

Capacitor 2: Measured inside a humidity-controlled chamber at fixed 500mV (rms), with humidity precisely set to 40%, 70% and 90%, over 0.1Hz to 100kHz. Temperature was maintained at 25°C.

2.3. Kramers-Kronig Validation

The physical consistency of the impedance data was evaluated using linear Kramers-Kronig (KK) transforms. Prior to Kramers–Kronig transformation, the measured impedance was converted to the passive sign convention, where a capacitive imaginary impedance is positive. The KK reconstruction was implemented using the discretized integral formulation proposed by Agarwal, Orazem, and García-Rubio [15]. The normalized root-mean-square error (NRMSE) were used as metrics to quantify deviation between measured and KK-reconstructed impedance.

Although the Kramers–Kronig relations formally require data over an infinite frequency range, the measured impedance spans six decades (0.1 Hz to 100 kHz), which is sufficient to assess relative consistency and identify humidity-induced deviations from ideal behavior within the frequency window of interest.

2.4. Formulation

The complex impedance Z over a given frequency range, is expressed in term of theirs real and imaginary parts as:

$$Z = Z' + jZ'' \tag{1}$$

The impedance can be expressed in terms of a complex permittivity, $\varepsilon = \varepsilon^{'} + j\varepsilon^{''}$, as

$$Z = \frac{1}{j\omega C} \tag{2}$$

where C is the complex capacitance:

$$C = \frac{A(\varepsilon' + j\varepsilon'')}{t}, \tag{3}$$

The relative (effective) dielectric permittivity is:

$$\varepsilon'_r = \frac{\varepsilon'}{\varepsilon_O} \tag{4}$$

where ε′ is the real permittivity, ε_O as the permittivity of free space.

The real permittivity can then be expressed as:

$$\varepsilon' = -\frac{t}{A}\frac{Z''}{\omega|Z|^2} \tag{5}$$

where ω is angular frequency, A is electrode area, t is film thickness, and $|Z|$ is magnitude of the complex impedance.

The imaginary part of the impedance can be expressed as:

$$Z'' = -\frac{t}{A\omega}\left(\frac{\varepsilon'}{\varepsilon'^2 + \varepsilon''^2}\right) \tag{6}$$

The loss tangent is a dimensionless metric that quantifies the fraction of the stored electrical energy dissipated as heat per AC cycle. It is defined as the ratio of the imaginary to the real parts of the complex permittivity:

 doi:10.20944/preprints202603.1699.v1

$$\tan\delta = \frac{\varepsilon''}{\varepsilon'} = \frac{Z'}{|Z''|} \tag{7}$$

The Kramers–Kronig (K–K) relations is used to verify the validity and consistency of the measured impedance data with the fundamental requirements of a linear, causal, and time-invariant system.

$$Z'_{kk} = Z'(\infty) + \frac{2}{\pi}\int_0^{\infty} \frac{wZ''(w) - \omega Z''(\omega)}{\omega^2 - w^2} dw \tag{8}$$

$$Z''_{kk} = -\frac{2}{\pi}\int_0^{\infty} \frac{\omega Z'(w) - \omega Z'(\omega)}{\omega^2 - w^2} dw \tag{9}$$

where $Z'(\infty)$ represents the series resistance of the device.

To discretize, the variable is changed to a logarithmic scale:

$$u = ln(w) \rightarrow du = \frac{dw}{w} \tag{10}$$

Evaluating at zero, the value of the new variable is:

$$u(0) = ln(0) = -\infty \tag{11}$$

At the infinite limit:

$$u(\infty) = ln(\infty) = \infty \tag{12}$$

The integrals can be written as:

$$Z'_{kk} = \frac{2}{\pi}\int_{-\infty}^{\infty} \frac{wwZ''(w) - w\omega Z''(\omega)}{w^2 - \omega^2} du \tag{13}$$

$$Z''_{kk} = -\frac{2}{\pi}\int_{-\infty}^{\infty} \frac{\omega wZ''(w) - \omega wZ''(\omega)}{w^2 - \omega^2} du \tag{14}$$

By discretizing the integral, the differential du becomes an increment Δu:

$$du = \Delta u = \Delta(\ln(w)) \tag{15}$$

Given ω_j=w, ω_i=ω , and using (13), the integrals can be approximated as a sum using the rectangle/trapezium rule in u:

$$Z'_{kk} = \frac{2}{\pi}\sum_{j\neq i} \frac{{\omega_j}^2 Z''(\omega_j) - \omega_j\omega_i Z''(\omega_i)}{{\omega_j}^2 - {\omega_i}^2} \Delta[ln(\omega_j)] \tag{16}$$

$$Z''_{kk} = -\frac{2}{\pi}\sum_{j\neq i} \frac{\omega_i\omega_j Z'(\omega_j) - \omega_i\omega_j Z'(\omega_i)}{{\omega_j}^2 - {\omega_i}^2} \Delta[ln(\omega_j)] \tag{17}$$

The value j=i is excluded because near w=ω the integrand becomes infinite. In electrical impedance spectroscopy, frequency often varies over many decades, so logarithmic spacing is convenient because it gives the same number of points per decade of frequency, and it also improves the numerical stability of the Kramers–Kronig formulas because the summation terms are more balanced.

 doi:10.20944/preprints202603.1699.v1

The residuals [13] are defined as:

$$\Delta Z' = \frac{|Z' - Z'_{rr}|}{|Z|} \tag{18}$$

$$\Delta Z'' = \frac{|Z'' - Z''_{rr}|}{|Z|} \tag{19}$$

Normalized Root Mean Square errors are normalized with respect to the value module measured at that point and are defined as:

$$NRMSE'_Z = 100\% \sqrt{\frac{1}{N}\sum_n \left(\frac{Z'(n) - Z'_{rr}(n)}{|Z(n)|}\right)^2} \tag{20}$$

$$NRMSE''_Z = 100\% \sqrt{\frac{1}{N}\sum_n \left(\frac{Z''(n) - Z''_{rr}(n)}{|Z(n)|}\right)^2} \tag{21}$$

2.5. Transmission Line Modeling (TLM)

To accurately capture the frequency response under high humidity, an augmented hybrid Transmission Line Model (TLM) was employed, as illustrated in Figure 1. This configuration divides the nanoparticle network into a bulk region and an interface region, each comprising discrete cells. Based on the impedance formalism for mixed ionic-electronic conductors (MIECs) [16], the bulk regions are characterized by distributed resistances (r_i , r_e) and chemical capacitances ($C_{\mu i}$, $C_{\mu e}$), while terminal impedances at the back and front contacts (C_{bi}, R_{bi}, C_{be}, R_{be}, C_{fi}, R_{fi}, C_{fe}, R_{fe}) account for interfacial charge transfer and reaction processes. The geometrical dielectric capacitance is represented by C_d. A key feature of this augmented model is the inclusion of parallel leakage resistances, R_{li} and R_{le}, across the ionic and electronic branches. These parameters account for shunt conduction paths—likely through condensed water bridges—that bypass the structured surface transport, providing a physical basis for the observed low-frequency impedance roll-off at high RH levels.

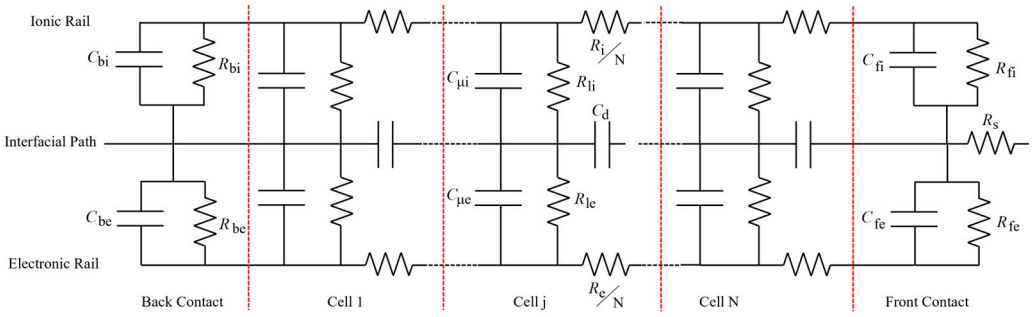

Figure 1. Augmented hybrid Transmission Line Model (TLM) for nanostructured silica MIM capacitor under high humidity. Two parallel rails represent ionic and electronic conduction, coupled by chemical capacitors. Terminal impedances account for charge transfer and electrochemical coupling at metal/water and water/SiO_2 interfaces. Leakage resistances (R_l) model shunt paths through condensed water bridges, capturing the humidity-induced transition from dielectric to mixed conduction behavior.

3. Results

3.1. SEM Characterization

 doi:10.20944/preprints202603.1699.v1

Figure 2 reports the cross-sectional SEM images of the fabricated devices with SiO_2 nanoparticles. The total thickness of the first electrosprayed nanoparticle dielectric layer (a) is 1.21 μm, meanwhile thicknesses of 0.3 μm and 1.0 μm are the bottom and top layer thicknesses respectively. The second nanostructure SiO_2 thickness is 3.11 μm with bottom layer of 0.6 μm and top layer of 1.2 μm.

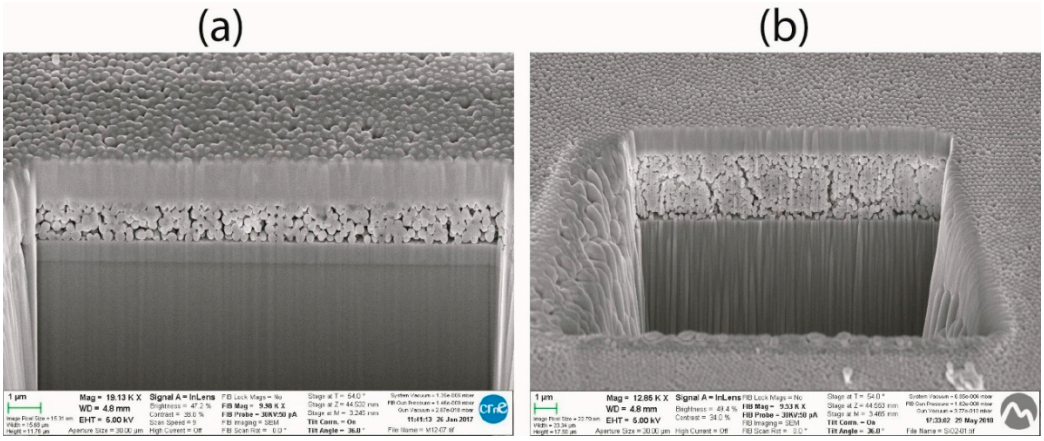

Figure 2. Drilled cross section SEM images of (a) First Electrosprayed SiO2 nanostructure, (b) Second Electrosprayed SiO2 nanostructure.

3.2. Capacitor-1: Dielectric Characteristics at Room Humidity

As shown in Figure 3(a), the silica capacitor incorporating nanoparticles exhibits a strong frequency-dependent dispersion of the relative permittivity (ε_r'). Log-log plot reveals exceptionally high low-frequency permittivity values, reaching approximately 1726 (at 500 mV) and 1568 (at 100 mV). A slight increase observed under 500 mV compared with 100 mV suggests a minor field-enhancement of interfacial polarization processes in the low frequency regime. When the frequency goes up, the permittivity falls very quickly by several orders of magnitude (109 at 1 kHz). Furthermore, above approximately 1 kHz, the permittivity is not affected by the excitation voltage, and stabilizes at a value of 51.1 at 1 MHz.

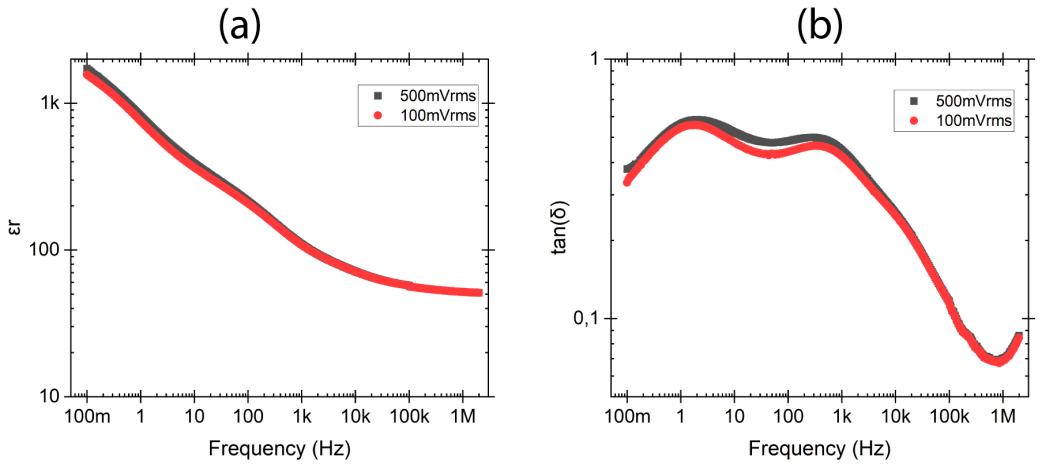

Figure 3. (a) Relative permittivity and (b) loss tangent for silica nanoparticles metal-insulator-metal capacitor.

This stabilized value remains significantly higher (13.1 times) than a conventional film bulk silica (~3.9). Conversely, at the lowest frequency, effective permittivity of the nanoparticles layers is 442.6 times higher than the effective permittivity of conventional silica. The extremely high values are attributed to the cumulative effect of polarization at the electrodes-dielectric interface, the interfaces between the nanoparticles themselves, and the presence of adsorbed moisture (which introduces

 doi:10.20944/preprints202603.1699.v1

mobile charge carriers) as mentioned in previous works. This response is therefore dominated by extrinsic residual interfacial and space-charge effects rather than intrinsic dielectric polarization.

Figure 3(b) shows the frequency dispersion of the loss tangent (tan δ) measured under 500 mV and 100 mV excitation voltages. The loss tangent exhibits a characteristic profile, with high values at low frequencies, reaching a maximum of approximately 0.58 at 2 Hz for 500mVrms. As the frequency increases, tan δ decreases steadily, reaching a minimum value of 0.067 at 0.85 MHz reached for 100mVrms, without exhibiting a clear plateau up to 1 MHz. A decreasing similar was observed in an Al/SiO_2/p-Si capacitor in the range from 50kHz to 1MHz [17]. Notably, a small voltage dependence is observed across the low-to-mid-frequency range (approximately 0.1 Hz to 2 kHz), where a higher applied voltage results in greater loss tangent.

This behavior suggests the presence of field-assisted, non-linear charge transport contribution [18] in addition to interfacial polarization processes. The overall shape of the tan δ dispersion, particularly the elevated losses at low frequencies, is characteristic of conductive losses dominated by leakage current [19] and interfacial polarization in porous homogenous silica nanostructure [20]. Consequently, the capacitor is significantly more efficient in terms of the relationship between stored and dissipated energy at high frequencies, where loss tangent is reduced. This trade-off highlights that the observed giant apparent permittivity at low frequencies is accompanied by significant energy dissipation, and therefore does not represent a high intrinsic dielectric energy storage capability of the silica material.

3.3. Capacitor 1: Impedance Consistency with Kramers-Kronig Integrals

The physical consistency of the impedance data was evaluated through Kramers-Kronig (KK) transforms implemented according to the formalism proposed by [21]. The KK validation yielded excellent agreement for the real part of the impedance, only at low frequency a small deviation between the measured and reconstructed impedance can be seen in Figure 4(a). The average residual was 2.13%, and the normalized root-mean-square error (NRMSE) was 3.3%. These low values confirm that the resistive component of the system satisfies the fundamental requirements of linearity, causality, and stability across the entire frequency range.

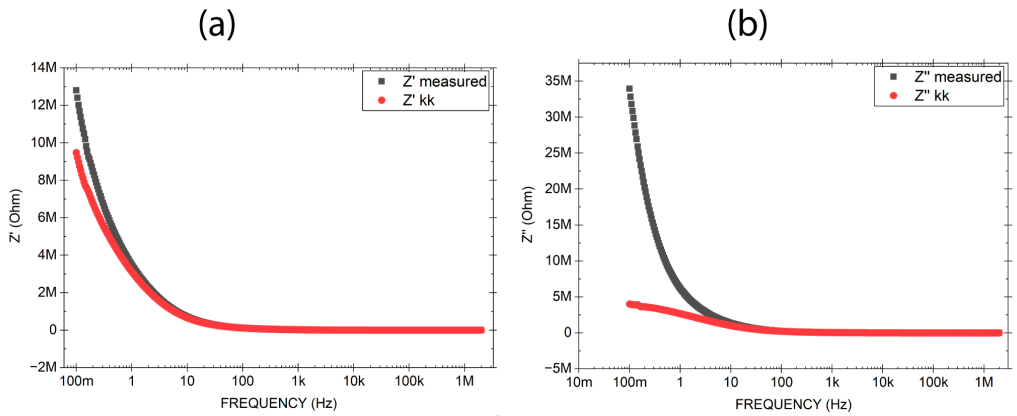

Figure 4. Spectrum comparison between the measured real and imaginary part of the impedance with the Kramers-Kronig (KK) impedances for an applied voltage of 500 mVrms: The Z''KK curve does not follow the Z' measured curve at low frequencies. .

In contrast, the imaginary part exhibits large deviation (Figure 4(b)), with an average residual of 18.13% and an NRMSE of 28.98%. Although these errors are significantly higher than those for Z′, they are not indicative of poor data quality. Instead, they reflect non-ideal physical processes inherent to porous and the moisture absorption nature of SiO_2 nanostructure (interfacial polarization and moisture-induced ionic conduction). These phenomena violate the strict Kramers-Kronig assumption, especially at low frequencies. Notably, when the KK integral is limited to the high

 doi:10.20944/preprints202603.1699.v1

frequency range (100 Hz - 2 MHz), the NRMSE for Z″ drops to 4.5%, confirming that the device behaves more linear and causal under conditions where polarization and conduction transients have insufficient time to develop.

Crucially, the high fidelity of the real-part validation reinforces the reliability of the measured impedance for dielectric analysis. It suggests that at high frequencies, the capacitor behavior is governed primarily by the intrinsic dielectric properties of silica, while the discrepancies of imaginary part at low frequencies faithfully capture the complex microstructural and environmental interactions of the material, rather than instrumental artifacts.

3.4. Capacitor 2: Dielectric Characteristic at Controlled Humidity

It is important to emphasize that Capacitor-2 differs from Capacitor-1 no only in electrode area and dielectric thickness, but also in the stochastic microstructure of the electrosprayed silica nanoparticle assemblies. Although relative permittivity and loss tangent are, in principle, independent of device geometry, the effective dielectric characteristics may be strongly influenced by factors such as particle packing density, pore connectivity, and interfacial are, which vary from device to device. Therefore, the present analysis is focused how controlled relative humidity systematically affects the dielectric response within a given device.

Figure 5(a) shows that increasing the relative humidity condition leads a marked enhancement of the effective permittivity. At 0.1Hz and 90% RH, the relative permittivity reaches a maximum value of 6870, approximately 1761 times higher than the intrinsic permittivity of bulk silica (~3.9), while at 0.1Hz and 40% RH, the maximum effective permittivity decreases to 2690. The extrinsic permittivity vanishes at high frequencies, where the response converges toward the intrinsic dielectric behavior. This confirm that water molecules into the nanostructure to provide ionic carriers (e.g., H^+ and OH^-) that increases interfacial polarization and increases the capacity to store charge.

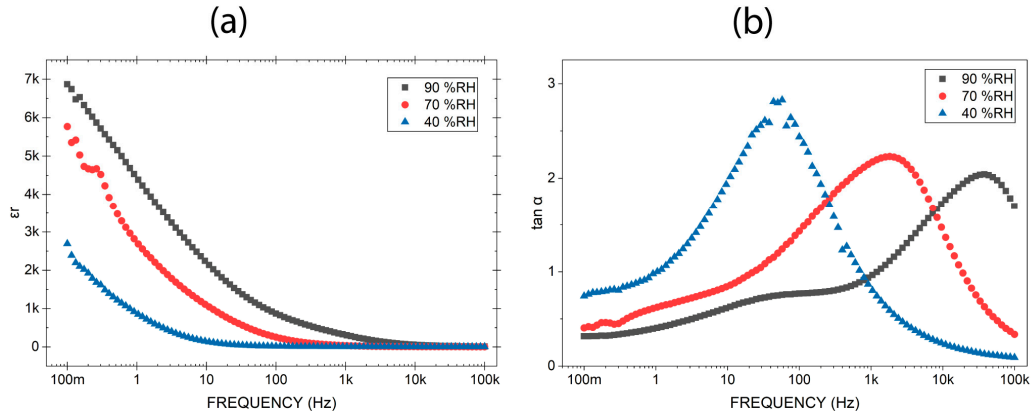

Figure 5. Effective permittivity (a) and loss tan δ (b) as a function of frequency measured at 90 %RH, 70% RH and 40% RH.

The Figure 5(b) reveals that loss tangent decreases with increasing relative humidity in the low frequency range (below 260 Hz). This trend reflects a relative enhancement in energy storage over dissipation, as the real permittivity (ε′) increases more rapidly than the imaginary permittivity (ε″). Consequently, the frequency range where tan δ < 1, indicating dominant capacitive behavior, expands toward lower frequencies under higher humidity. The reduction of tan δ at high humidity reflects a faster increase of ε′ relative to ε″, rather than a reduction of dissipative processes. At high frequencies (above 10kHz), tan δ increases because the permittivity ε′ diminish as interfacial polarization can no longer follow the rapidly alternating field.

3.5. Capacitor 2: Effect of Relative Humidity on the Kramers–Kronig Validation of Impedance Spectra for an Electrosprayed Silica Nanostructure

 doi:10.20944/preprints202603.1699.v1

It should be noted that two MIM capacitors analyzed in this study differ in both electrodes area and dielectric thickness, resulting in distinct absolute impedance values. Therefore, the following analysis focuses on the qualitative trends associated by humidity, rather than direct quantitative comparison between devices.

The real part of the impedance under controlled relative humidity is showed in Figure 5(a). As the humidity increase, the real part of the impedance decreases and deviates from the impedance obtained by Kramers-Kronig transform at low frequencies. The normalized root-mean-square (NRMSE) for Z′ was 141.2%, 94.5% and 14.5% at 90%RH, 70%RH and 40%RH respectively. This increasing divergence, particularly at elevated humidity levels and in the low-frequency data, suggests a failure to meet the conditions of linearity and causality required for KK validity.

In Figure 6(a), the reduction in Z′ with increasing humidity is attributed to the absorption of water humidity into the porous electrospray silica layer, indicating that moisture-induced introduce time-dependent effects that prevent strict Kramers-Kronig consistency, particularly in the low-frequency range. This absorption phenomena enhances ionic conductivity across the dielectric, effectively lowering the overall resistive component of the impedance. In other words, moisture transforms the insulating silica nanostructure into a partially conductive medium, thereby reducing the real part of the impedance.

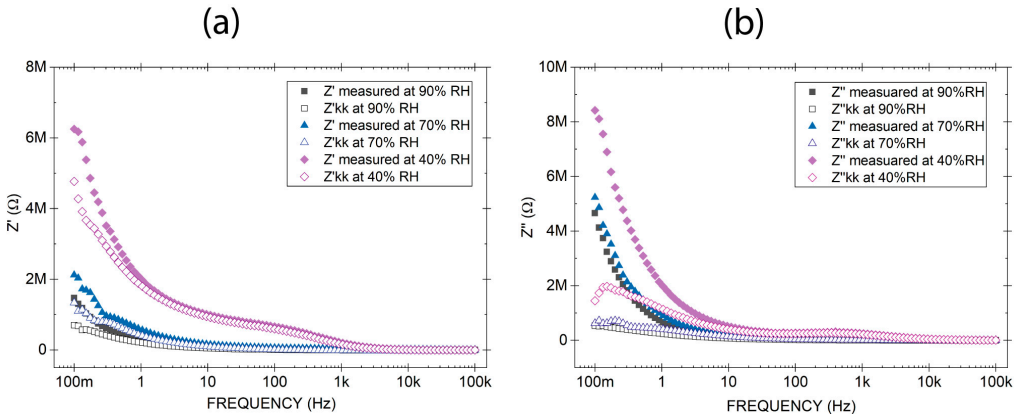

Figure 6. Comparison between measured and Kramers–Kronig reconstructed real (left) and imaginary (right) parts of impedance for an electrosprayed silica MIM capacitor under controlled relative humidity conditions (90% RH, 70% RH, and 40% RH). It demonstrates that increasing humidity progressively destroys KK consistency at low frequencies, indicating the emergence of slow ionic and interfacial processes incompatible with linear time-invariant assumptions.

The imaginary component of the impedance, Z″, exhibits values decreasing as humidity increases (Figure 6(b)). At 1 Hz, for instance, Z″ is approximately 658 kΩ at 90% RH, 899 kΩ at 70% RH, and 1.9 MΩ at 40% RH. This trend, where higher humidity leads to lower Z″, is consistent with the strong increase in effective permittivity (ε′) due to interfacial polarization enhanced by water adsorption in the porous silica structure. Since Z″ is proportional to ε′ and inversely proportional to $(\varepsilon')^2+(\varepsilon'')^2$, as humidity increases, both ε′ and ε″ rise due to interfacial polarization and ionic conduction, but ε′ grows more than ε″, causing Z″ to decrease. Thus, the reduction in Z″ reflects the dominance of enhanced charge storage (high ε′) over dissipative processes, consistent with the observed decrease in tan δ (Figure 4(b)), which indicates improved energy storage efficiency despite the presence of ionic conduction.

The Kramers–Kronig validation further supports this interpretation: the normalized RMS error for Z″ reaches 51.6% at 90% RH, indicating significant deviation from linearity and causality due to non-ideal effects such as ionic conduction and interfacial polarization. In contrast, at 40% RH, the NRMS error drops to 27.1%, reflecting a more "ideal" capacitive behavior.

3.6. Capacitor 2: Physical Interpretation via TLM Fitting

 doi:10.20944/preprints202603.1699.v1

As illustrated in Figure 7, the TLM model accurately captures the Nyquist and Bode responses across different relative humidity levels. The evolution of the fitted parameters (Figure 7(d)) shows a great shift. The characteristic resistances of the network: total ionic and electronic resistance (Ri, Re), leakage ionic resistance (Rli) and ionic front contact resistance (Rfi), exhibit a synchronized decrease of approximately three orders of magnitude. This coordinated reduction suggests that moisture does not only increase the number of charge carriers but fundamentally enhances the global connectivity of the ionic network through the percolation of adsorbed water layers. The complete set of fitted parameters is provided in Supplementary Table S1. While some terminal elements exhibited extreme values indicative of overparameterization in those specific branches (commons in distributed element models with multiple interfacial processes), bulk and leakage resistances show robust convergence.

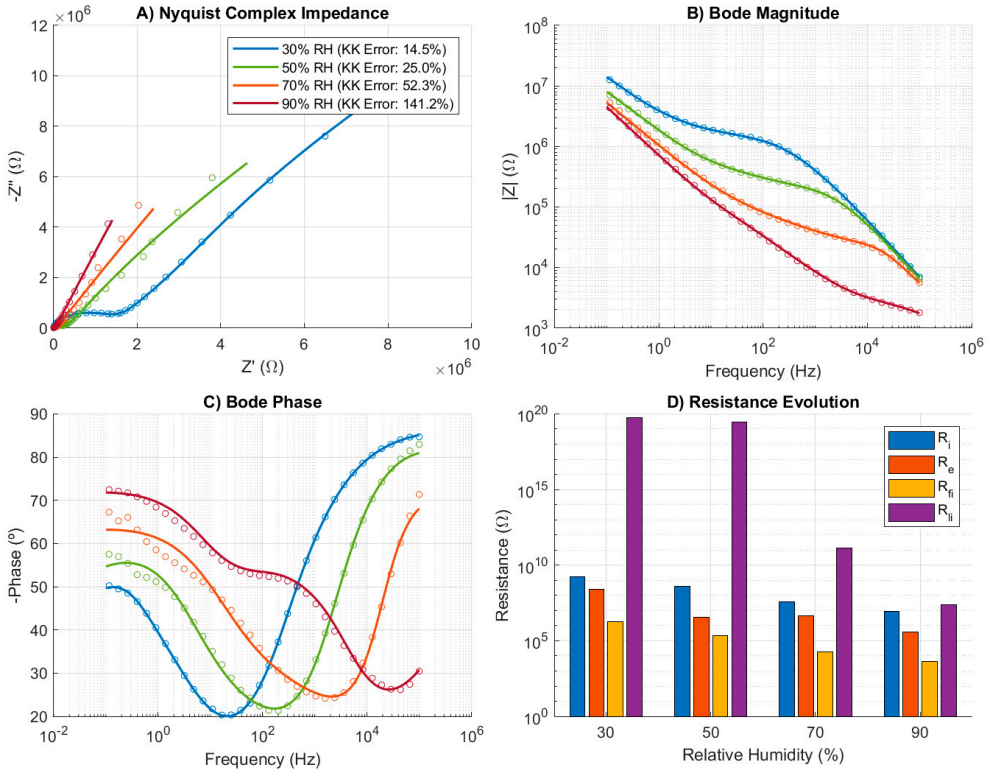

Figure 7. Transmission Line Model (TLM) fitting results for the nanostructured silica MIM capacitor under controlled relative humidity (30–90% RH). (a–c) Nyquist and Bode plots showing experimental impedance data (symbols) and TLM fits (solid lines) at representative humidity levels. (d) Evolution of key fitted parameters.

4. Discussion

The exceptionally high effective permittivity, 1726 for the nanostructured silica capacitor-1, and 2690 for the nanostructured silica capacitor-2 (at 40 %RH), observed at low frequencies is a macroscopic response controlled by interfacial polarization [22]. This phenomenon, often referred to as Maxwell-Wagner-Sillar (MWS) polarization in composite systems, arises from accumulation of free charge at internal interfaces or phase boundaries with contrasting electrical conductivities. In our case, it physically originates from space-charge accumulation within the nanoporous silica network and at the electrode interface, and moisture-assisted ionic transport within nanoporous electrosprayed structure, rather than an inherent characteristic of SiO_2. It is evident that slow polarization mechanisms predominate in the low-frequency zone due to the fast collapse of ε_r' with frequency (ε_r' = 51.1 at 1MHz for capacitor-1) and the substantial dependency on humidity and excitation voltage.

The frequency-dependent giant permittivity observed in the present work is consistent with previous reports on nanostructured silica dielectrics, notably the study by Sakthisabarimoorthi et al. [9], where large dielectric constants (e.g., 2368 at 1 Hz and 40°C, dropping to ε_r' = 68 at 1 MHz) were

 doi:10.20944/preprints202603.1699.v1

attributed to interfacial polarization and charge accumulation within porous SiO_2 networks. Similar to their observations, the enhancement is confined to the low-frequency regime and rapidly diminishes at higher frequencies, indicating the dominance of slow polarization mechanisms. Despite the strong dependence of permittivity on effective microstructure, a close agreement is observed with the dielectric response reported by Sakthisabarimoorthi et al. for silica nanostructures fabricated using a different processing route, providing independent and robust validation that the observed giant permittivity is an extrinsic artifact, overwhelmingly dominated by interfacial polarization rather than an intrinsic property of silica.

The reduction in tan δ with humidity at low frequencies (Figure 4(b)) is not indicative of lower absolute dissipation, but rather of a relative increase in energy storage capacity (ε′) compared to losses (ε″). Thus, while the system becomes more efficient in terms of the ratio of stored to dissipated energy, the absolute energy loss remains significant. Although moisture causes the presence of a larger population of mobile ionic species, and therefore an increase in imaginary component ε″ associated with conductive losses, in the low-frequency regime, ionic motion remains partially blocked, contributing predominantly to energy storage rather than dissipation. At higher frequencies (above 10kHz), this balance reverses, the interfacial polarization can no longer follow the rapidly alternating, causing ε′ to drop, thereby increasing tan δ.

This crossover behavior contrasts with the temperature-dependent trends reported by Sakthisabarimoorthi et al. While Sakthisabarimoorthi observed a reduction in tan δ with increasing temperature in a dry environment, our study examines that the effect of increasing relative humidity at constant temperature, is a decreasing in tan δ. In their case, thermal activation enhances charge mobility without introducing additional interfacial water layers, whereas in our system, humidity promotes the formation of hydrated interfaces that improved the interfacial polarization. The apparent discrepancy thus reflects distinct dominant mechanisms under humidity-controlled versus thermally driven conditions, rather than a contradiction, and further supports the interpretation that the giant permittivity in nanostructured silica is governed by extrinsic interfacial effects strongly modulated by environmental factors.

The Kramers–Kronig analysis reveals a fundamental distinction between measurements performed under ambient conditions and those under controlled humidity. While the ambient-condition capacitor shows excellent KK consistency for Z′, increasing relative humidity progressively destroys KK validity at low frequencies. This behavior does not indicate experimental artifacts, but rather the emergence of time-dependent and history-dependent processes, such as ionic drift and electrode polarization, which violate the assumptions of linear time-invariant systems.

The breakdown of Kramers-Kronig (KK) consistency at high RH (NRMSE > 100%) correlates with the abrupt activation of leakage paths. At 90% RH, Rli falls significantly (to $2.3 \times 10^{+7}$ Ω), becoming a dominant conduction mechanism. This suggests that the 'Giant Permittivity' measured at low frequencies is heavily influenced by a quasi-DC ionic shunt. Since KK transforms assume a linear, causal, and stationary dielectric response, the emergence of these humidity-induced conduction channels and interfacial charge accumulation introduces non-linearities that invalidate the KK assumptions, confirming that the massive increase in effective capacitance is coupled with a fundamental change in the transport regime.

From an application standpoint, these findings highlight a fundamental trade-off. While humidity dramatically enhances apparent permittivity, it simultaneously introduces non-ideal effects that compromise physical consistency and long-term stability. Therefore, electrosprayed silica nanostructures are highly attractive for humidity sensing applications, but require strict environmental control when employed as stable dielectrics in energy storage or microelectronic devices.

5. Conclusions

This study demonstrates that ambient humidity profoundly influences both the impedance response and the physical validity of Kramers–Kronig (KK) transforms in nanoporous electrosprayed

 doi:10.20944/preprints202603.1699.v1

SiO_2 MIM capacitors. In this work, Kramers–Kronig consistency is not interpreted here as a binary validity criterion, but rather as a sensitive probe of hidden non-idealities. Deviations from KK relations are used to identify the emergence of non-linear, non-stationary, or history-dependent processes, particularly those associated with moisture-induced ionic conduction and interfacial polarization in nanostructured SiO_2. Two distinct devices were characterized using impedance spectroscopy and analyzed:

Capacitor 1, measured under ambient conditions, exhibited excellent KK consistency for the real part of impedance (NRMSE=3.3%). Nevertheless, the imaginary component shows larger deviations (NRMSE=28.98%) compared to the real part, but this does not imply poor data quality. These differences arise from non-ideal physical effects in silica nanostructures, such as moisture absorption and interfacial polarization.

Capacitor 2, tested under controlled RH, showed a dramatic degradation in KK validity as humidity increased: NRMSE for Z′ escalated from 14.5% at 40% RH to 141.2% at 90% RH, directly attributable to moisture induced ionic conduction and interfacial polarization. Meanwhile, imaginary part of the impedance decreased with rising humidity, a behavior consistent with the increase in dielectric losses due to enhanced bulk conductivity.

The measurements of permittivity and dielectric losses are valid as a representation of the macroscopic response of the device under the given experimental conditions. However, they should not be interpreted as intrinsic properties of silicon oxide, but rather as manifestations of non-linear extrinsic effects such as moisture absorption, interfacial polarization, and ionic conduction.

Furthermore, the Transmission Line Modeling (TLM) analysis corroborates these findings by revealing a synchronized three-order of magnitude reduction in network resistance at high humidity, confirming that adsorbed water molecules form interconnected conductive pathways across the nanoparticles network, enabling ionic conduction at high relative humidity.

Finally, for practical applications, these findings imply that electrosprayed silica structures are highly suitable for humidity-sensing platforms, but require strict environmental control when employed as stable dielectrics in energy storage or integrated circuits.

Supplementary Materials: The following supporting information can be downloaded at the website of this paper posted on Preprints.org, Table S1: Fitted parameters of the augmented hybrid Transmission Line Model (TLM).

Author Contributions: Conceptualization, B.V. and S.B.; methodology, B.V. and A.O.; validation, B.V., A.O. and M.D.-P.; formal analysis, B.V., A.O., and S.B; investigation, B.V. and A.O; resources, S.B.; writing—original draft preparation, B.V.; writing—review and editing, B.V., A.O., S.B. and M.D.-P.; visualization, B.V.; supervision, S.B.; project administration, S.V.; funding acquisition, M.D.-P. and S.V.; All authors have read and agreed to the published version of the manuscript.

Funding: This research was funded by Spanish Ministry MICIN under grant number PID2024-161247OB-C32 and CPP2023-010559, and by INCYT under grant number CUP 91870000.0000.390370.

Institutional Review Board Statement: Not applicable.

Informed Consent Statement: Not applicable.

Data Availability Statement: The original contributions presented in this study are included in the article. Raw and processed data are available at: Véliz, Bremnen (2026), "Data Set of Impedance Spectroscopy Data and Physical Consistency of Humid Nanostructured Silica MIM Capacitors", Mendeley Data, V1, doi: 10.17632/kkhnp375ds.1.

Conflicts of Interest: The authors declare no conflicts of interest.

References

 doi:10.20944/preprints202603.1699.v1

1. Yan, Y.; Kilchytska, V.; Wang, B.; Faniel, S.; Zeng, Y.; Raskin, J.P.; Flandre, D. Characterization of Thin Al2O3/SiO2 Dielectric Stack for CMOS Transistors. *Microelectron. Eng.* **2022**, *254*, doi:10.1016/j.mee.2022.111708.
2. Palumbo, F.; Wen, C.; Lombardo, S.; Pazos, S.; Aguirre, F.; Eizenberg, M.; Hui, F.; Lanza, M. A Review on Dielectric Breakdown in Thin Dielectrics: Silicon Dioxide, High-k, and Layered Dielectrics. *Adv. Funct. Mater.* 2020, *30*.
3. Chen, H.Y.; Li, S.S.; Li, M.H. A Low Impedance CMOS-MEMS Capacitive Resonator Based on Metal-Insulator-Metal (MIM) Capacitor Structure. *IEEE Electron Device Letters* **2021**, *42*, 1045–1048, doi:10.1109/LED.2021.3081365.
4. Austin, D.Z.; Allman, D.; Price, D.; Hose, S.; Conley, J.F. Plasma Enhanced Atomic Layer Deposition of Al2O3 /SiO2 MIM Capacitors. *Ieee Electron Device Letters* **2015**, *36*, 496–498, doi:10.1109/LED.2015.2412685.
5. Park, J.S.; Sheng, J.; Han, J.H.; Choi, W.H.; Park, J. Performance and Stability Enhancement of In-Sn-Zn-O TFTs Using SiO2 Gate Dielectrics Grown by Low Temperature Atomic Layer Deposition. *ACS Appl. Mater. Interfaces* **2017**, *9*, 42928–42934, doi:10.1021/acsami.7b15419.
6. Liu, L.L.; Morgan, S.P.; Correia, R.; Korposh, S. A Single-Film Fiber Optical Sensor for Simultaneous Measurement of Carbon Dioxide and Relative Humidity. *Opt. Laser Technol.* **2022**, *147*, doi:10.1016/j.optlastec.2021.107696.
7. Véliz, B.; Bermejo, S.; Orpella, A.; Castañer, L. Impedance Modeling of Silica Nanoparticle Metal Insulator Metal Capacitors. *Electrochim. Acta* **2018**, *280*, 62–70, doi:10.1016/j.electacta.2018.05.084.
8. E. Barsoukov, J.R.M. *Impedance Spectroscopy: Theory, Experiment, and Applications*; Second.; John Wiley & Sons, 2005; ISBN 0471647497.
9. Sakthisabarimoorthi, A.; Martin Britto Dhas, S.A.; Jose, M. Electrical Impedance Spectroscopic Investigations of Monodispersed SiO2 Nanospheres. *Superlattices Microstruct.* **2018**, *113*, 271–282, doi:10.1016/j.spmi.2017.11.001.
10. Véliz, B.; Orpella, A.; Domiguez-Pumar, M.; Bermejo, S. *Analysis and Impedance Modeling of Silica and Polystyrene Nanoparticles in EMIM Structures for Humidity Sensing Applications*; 2024; Vol. 22;.
11. Véliz, B.; Bermejo, S.; Coll, A.; Castañer, L. Metal-Insulator-Metal Capacitor Using Electrosprayed Nanoparticles. *Appl. Phys. Lett.* **2014**, *105*, doi:10.1063/1.4889746.
12. Boukamp, B.A. A Linear Kronig-Kramers Transform Test for Immittance Data Validation. *J. Electrochem. Soc.* **1995**, *142*, doi:10.1149/1.2044210.
13. Schönleber, M.; Klotz, D.; Ivers-Tiffée, E. A Method for Improving the Robustness of Linear Kramers-Kronig Validity Tests. *Electrochim. Acta* **2014**, *131*, 20–27, doi:10.1016/j.electacta.2014.01.034.
14. Luo, J.; Liang, X.; Zhang, Y.; Liang, C.; Yassine, H.; Leroy, G.; Carru, J.C.; Mascot, M. Application of the Kramers–Kronig Relationships in the Electrochemical Impedance Models Fit. *Journal of Solid State Electrochemistry* **2021**, *25*, 2225–2233, doi:10.1007/s10008-021-04975-1.
15. Agarwal Pankai; Orazem Mark E.; Garcia-Rubio Luis H. Application of the Kramers-Kronig Relations in Electrochemical Impedance Spectroscopy. In *Electrochemical Impedance: Analysis and Interpretation*; ASTM International, 1993; Vol. STP1188, pp. 115–139.
16. Bumberger, A.E.; Nenning, A.; Fleig, J. Transmission Line Revisited - the Impedance of Mixed Ionic and Electronic Conductors. *Physical Chemistry Chemical Physics* 2024, *26*, 15068–15089.
17. Tataroğlu, A.; Altindal, Ş.; Bülbül, M.M. Temperature and Frequency Dependent Electrical and Dielectric Properties of Al/SiO2/p-Si (MOS) Structure. *Microelectron. Eng.* **2005**, *81*, 140–149, doi:10.1016/j.mee.2005.04.008.
18. Bheesayagari, C.R.; Pons-Nin, J.; Orpella, A.; Véliz, B.; Bermejo, S.; Domínguez-Pumar, M. Conduction Mechanisms and Charge Trapping Control in SiO2 Nanoparticle MIM Capacitors. *Electrochim. Acta* **2020**, *346*, doi:10.1016/j.electacta.2020.136202.
19. Harrell, W.R.; Frey, J. Observation of Poole-Frenkel Effect Saturation in SiO 2 and Other Insulating Films. *Thin Solid Films* **1999**, *352*, 195–204, doi:https://doi.org/10.1016/S0040-6090(99)00344-2.
20. Qin, M.; Zhang, L.; Wu, H. Dielectric Loss Mechanism in Electromagnetic Wave Absorbing Materials. *Advanced Science* 2022, *9*.

 doi:10.20944/preprints202603.1699.v1

21. Orazem Mark E.; Tribollet Bernard *ELECTROCHEMICAL IMPEDANCE SPECTROSCOPY*; The Electrochemical Society Series, Ed.; A John Wiley & Sons, INC., 2008; ISBN 978-0-470-04140-6.
22. Ahmed Althumairi, N.; Hjiri, M.; Aldukhayel, A.M.; Jbeli, A.; Nassar, K.I. Recent Advances in Dielectric and Ferroelectric Behavior of Ceramic Nanocomposites: Structure Property Relationships and Processing Strategies. *Nanomaterials* 2025, *15*.